



**HAL**  
open science

## **Radiation resistant fiber Bragg grating in random air-line fibers for sensing applications in nuclear reactor cores**

Mohamed A.S. Zaghoul, Mohan Wang, Sheng Huang, Cyril Hnatovsky, Dan Grobnic, Stephen Mihailov, Ming-Jun Li, David Carpenter, Lin-Wen Hu, Joshua Daw, et al.

► **To cite this version:**

Mohamed A.S. Zaghoul, Mohan Wang, Sheng Huang, Cyril Hnatovsky, Dan Grobnic, et al.. Radiation resistant fiber Bragg grating in random air-line fibers for sensing applications in nuclear reactor cores. *Optics Express*, 2018, 26 (9), pp.11775-11786. 10.1364/OE.26.011775 . cea-01919455

**HAL Id: cea-01919455**

**<https://cea.hal.science/cea-01919455>**

Submitted on 18 Jan 2020

**HAL** is a multi-disciplinary open access archive for the deposit and dissemination of scientific research documents, whether they are published or not. The documents may come from teaching and research institutions in France or abroad, or from public or private research centers.

L'archive ouverte pluridisciplinaire **HAL**, est destinée au dépôt et à la diffusion de documents scientifiques de niveau recherche, publiés ou non, émanant des établissements d'enseignement et de recherche français ou étrangers, des laboratoires publics ou privés.



## NRC Publications Archive Archives des publications du CNRC

### **Radiation resistant fiber Bragg grating in random air-line fibers for sensing applications in nuclear reactor cores**

Zaghloul, Mohamed A.S.; Wang, Mohan; Huang, Sheng; Hnatovsky, Cyril; Grobnic, Dan; Mihailov, Stephen; Li, Ming-Jun; Carpenter, David; Hu, Lin-Wen; Daw, Joshua; Laffont, Guillaume; Nehr, Simon; Chen, Kevin P.

This publication could be one of several versions: author's original, accepted manuscript or the publisher's version. / La version de cette publication peut être l'une des suivantes : la version prépublication de l'auteur, la version acceptée du manuscrit ou la version de l'éditeur.

For the publisher's version, please access the DOI link below. / Pour consulter la version de l'éditeur, utilisez le lien DOI ci-dessous.

#### **Publisher's version / Version de l'éditeur:**

<https://doi.org/10.1364/OE.26.011775>

*Optics Express*, 26, 9, pp. 11775-11786, 2018

#### **NRC Publications Record / Notice d'Archives des publications de CNRC:**

<https://nrc-publications.canada.ca/eng/view/object/?id=de60c7d6-3da6-4c49-91a0-5f9013173767>

<https://publications-cnrc.canada.ca/fra/voir/objet/?id=de60c7d6-3da6-4c49-91a0-5f9013173767>

Access and use of this website and the material on it are subject to the Terms and Conditions set forth at

<https://nrc-publications.canada.ca/eng/copyright>

READ THESE TERMS AND CONDITIONS CAREFULLY BEFORE USING THIS WEBSITE.

L'accès à ce site Web et l'utilisation de son contenu sont assujettis aux conditions présentées dans le site

<https://publications-cnrc.canada.ca/fra/droits>

LISEZ CES CONDITIONS ATTENTIVEMENT AVANT D'UTILISER CE SITE WEB.

**Questions?** Contact the NRC Publications Archive team at

PublicationsArchive-ArchivesPublications@nrc-cnrc.gc.ca. If you wish to email the authors directly, please see the first page of the publication for their contact information.

**Vous avez des questions?** Nous pouvons vous aider. Pour communiquer directement avec un auteur, consultez la première page de la revue dans laquelle son article a été publié afin de trouver ses coordonnées. Si vous n'arrivez pas à les repérer, communiquez avec nous à PublicationsArchive-ArchivesPublications@nrc-cnrc.gc.ca.





# Radiation resistant fiber Bragg grating in random air-line fibers for sensing applications in nuclear reactor cores

MOHAMED A.S. ZAGHLOUL,<sup>1</sup> MOHAN WANG,<sup>1</sup> SHENG HUANG,<sup>1</sup> CYRIL HNATOVSKY,<sup>2</sup> DAN GROBNIC,<sup>2</sup> STEPHEN MIHAILOV,<sup>2</sup> MING-JUN LI,<sup>3</sup> DAVID CARPENTER,<sup>4</sup> LIN-WEN HU,<sup>4</sup> JOSHUA DAW,<sup>5</sup> GUILLAUME LAFFONT,<sup>6</sup> SIMON NEHR,<sup>6</sup> AND KEVIN P. CHEN<sup>1,\*</sup>

<sup>1</sup>Department of Electrical and Computer Engineering, University of Pittsburgh, Pittsburgh, PA 15261, USA

<sup>2</sup>National Research Council Canada, 100 Sussex Drive, Ottawa, ON K1A 0R6, Canada

<sup>3</sup>Corning Research and Development Corporation, Corning, NY 14831, USA

<sup>4</sup>MIT Nuclear Reactor Laboratory, 138 Albany Street, Cambridge, MA 02139, USA

<sup>5</sup>Idaho National Laboratory, 2525 Fremont Avenue, Idaho Falls, ID 83402, USA

<sup>6</sup>CEA, LIST, Laboratoire Capteurs et Architectures Electroniques, F-91191 Gif-sur-Yvette, France

\*pec9@pitt.edu

**Abstract:** This paper reports the testing results of radiation resistant fiber Bragg grating (FBG) in random air-line (RAL) fibers in comparison with FBGs in other radiation-hardened fibers. FBGs in RAL fibers were fabricated by 80 fs ultrafast laser pulse using a phase mask approach. The fiber Bragg gratings tests were carried out in the core region of a 6 MW MIT research reactor (MITR) at a steady temperature above 600°C and an average fast neutron (>1 MeV) flux  $>1.2 \times 10^{14}$  n/cm<sup>2</sup>/s. Fifty five-day tests of FBG sensors showed less than 5 dB reduction in FBG peak strength after over  $1 \times 10^{20}$  n/cm<sup>2</sup> of accumulated fast neutron dose. The radiation-induced compaction of FBG sensors produced less than 5.5 nm FBG wavelength shift toward shorter wavelength. To test temporal responses of FBG sensors, a number of reactor anomaly events were artificially created to abruptly change reactor power, temperature, and neutron flux over short periods of time. The thermal sensitivity and temporal responses of FBGs were determined at different accumulated doses of neutron flux. Results presented in this paper reveal that temperature-stable Type-II FBGs fabricated in radiation-hardened fibers can survive harsh in-pile conditions. Despite large parameter drift induced by strong nuclear radiation, further engineering and innovation on both optical fibers and fiber devices could lead to useful fiber sensors for various in-pile measurements to improve safety and efficiency of existing and next generation nuclear reactors.

© 2018 Optical Society of America under the terms of the [OSA Open Access Publishing Agreement](#)

**OCIS codes:** (060.2370) Fiber optics sensors; (060.3735) Fiber Bragg gratings; (350.5610) Radiation.

## References and links

1. P. Ferdinand, S. Magne, V. Dewynter-Marty, C. Martinez, S. Rougeault, and M. Bugaud, "Applications of Bragg grating sensors in Europe," in *Optical Fiber Sensors* (1997), paper OTuB1.
2. S. J. Mihailov, "Fiber Bragg grating sensors for harsh environments," *Sensors (Basel)* **12**(2), 1898–1918 (2012).
3. A. Gusarov and S. K. Hoeffgen, "Radiation effects on fiber gratings," *IEEE Trans. Nucl. Sci.* **60**(3), 2037–2053 (2013).
4. A. F. Fernandez, A. I. Gusarov, S. Bodart, K. Lammens, F. Berghmans, M. Decréton, P. Mégret, M. Blondel, and A. Delchambre, "Temperature monitoring of nuclear reactor cores with multiplexed fiber Bragg grating sensors," *Opt. Eng.* **41**(6), 1246–1254 (2002).
5. A. Gusarov, A. F. Fernandez, S. Vasiliev, O. Medvedkov, M. Blondel, and F. Berghmans, "Effect of gamma-neutron nuclear reactor radiation on the properties of Bragg gratings written in photosensitive Ge-doped optical fiber," *Nuclear Instrum. Methods. Phys. Res. Section B* **187**(1), 79–86 (2002).
6. A. Gusarov, "Long-term exposure of fiber Bragg gratings in the BR1 low-flux nuclear reactor," *IEEE Trans. Nucl. Sci.* **57**(4), 2044–2048 (2010).

7. A. F. Fernandez, A. Gusarov, B. Brichard, M. Decréton, F. Berghmans, P. Mégret, and A. Delchambre, "Long-term radiation effects on fibre Bragg grating temperature sensors in a low flux nuclear reactor," *Meas. Sci. Technol.* **15**(8), 1506–1511 (2004).
8. A. F. Fernandez, B. Brichard, F. Berghmans, and M. Decreton, "Dose-rate dependencies in gamma-irradiated fiber Bragg grating filters," *IEEE Trans. Nucl. Sci.* **49**(6), 2874–2878 (2002).
9. A. I. Gusarov, F. Berghmans, A. F. Fernandez, O. Deparis, Y. Defosse, D. Starodubov, M. Decreton, P. Mégret, and M. Bondel, "Behavior of fibre Bragg gratings under high total dose gamma radiation," *IEEE Trans. Nucl. Sci.* **47**(3), 688–692 (2000).
10. A. I. Gusarov, F. Berghmans, O. Deparis, A. F. Fernandez, Y. Defosse, P. Mégret, M. Decréton, and M. Blondel, "High total dose radiation effects on temperature sensing fiber Bragg gratings," *IEEE Photonics Technol. Lett.* **11**(9), 1159–1161 (1999).
11. R. S. Fielder, D. Klemmer, and K. L. Stinson-Bagby, "High neutron fluence survivability testing of advanced fiber Bragg grating sensors," *AIP Conf. Proc.* **699**(1), 650–657 (2004).
12. L. Remy, G. Cheymol, A. Gusarov, A. Morana, E. Marin, and S. Girard, "Compaction in optical fibres and fibre Bragg gratings under nuclear reactor high neutron and gamma fluence," *IEEE Trans. Nucl. Sci.* **63**(4), 2317–2322 (2016).
13. [https://www.corning.com/media/worldwide/coc/documents/Fiber/PI1445\\_07\\_14\\_English.pdf](https://www.corning.com/media/worldwide/coc/documents/Fiber/PI1445_07_14_English.pdf)
14. A. Morana, S. Girard, E. Marin, C. Marcandella, S. Rizzolo, J. Périsset, J. R. Macé, A. Taouri, A. Boukenter, M. Cannas, and Y. Ouerdane, "Radiation vulnerability of fiber Bragg gratings in harsh environments," *J. Lightwave Technol.* **33**(12), 2646–2651 (2015).
15. D. C. Bookbinder, R. M. Fiocco, M. J. Li, M. T. Murtagh, and P. Tandon, "Microstructured optical fibers and methods," U.S. Patent 7,450,806 (2008).
16. M. J. Li, P. Tandon, D. C. Bookbinder, D. A. Nolan, S. R. Bickham, M. A. McDermott, R. B. Desorcie, J. J. Englebert, S. L. Logunov, V. Kozlov, and J. A. West, "Nano-engineered optical fibers and applications," in *Optical Fiber Communication Conference* (2010), paper OWA2.
17. A. Cusano, A. Cutolo, and J. Albert, *Fiber Bragg Grating Sensors: Recent Advancements, Industrial Applications and Market Exploitation* (Bentham Science Publishers, 2011).
18. H. Henschel, J. Kuhnhen, and U. Weinand, "September. High radiation hardness of a hollow core photonic bandgap fiber," in *8th European Conference Radiation and Its Effects on Components and Systems* (2005) paper LN4-1.
19. C. Smelser, S. Mihailov, and D. Grobnc, "Formation of Type I-IR and Type II-IR gratings with an ultrafast IR laser and a phase mask," *Opt. Express* **13**(14), 5377–5386 (2005).
20. C. Hnatovsky, R. S. Taylor, P. P. Rajeev, E. Simova, V. R. Bhardwaj, D. M. Rayner, and P. B. Corkum, "Pulse duration dependence of femtosecond-laser-fabricated nanogratings in fused silica," *Appl. Phys. Lett.* **87**(1), 014104 (2005).
21. S. J. Mihailov, C. Hnatovsky, D. Grobnc, K. Chen, and M. J. Li, "Fabrication of Bragg Gratings in Random Air-Line Clad Microstructured Optical Fiber," *IEEE Photonics Technol. Lett.* **30**(2), 209–212 (2018).
22. A. Gusarov, D. Kinet, C. Caucheteur, M. Wuilpart, and P. Mégret, "Gamma radiation induced short-wavelength shift of the Bragg peak in Type I fiber gratings," *IEEE Trans. Nucl. Sci.* **57**(6), 3775–3778 (2010).

## 1. Introduction

Nuclear reactors are reliable and low-cost, carbon-free energy sources to supplement intermittent renewable energy production tied to the electrical grid. High spatial resolution and multi-modal information gathering sensors through the nuclear power system could have potentials to reduce design redundancy, and subsequently the overall cost of the nuclear power systems. Thus, development and implementation of radiation-hardened advanced sensors in reactor cores is a major theme for the development of next generation nuclear power systems. To ensure operational safety, multiple-level redundancies are built into nuclear reactors. These fail-safe designs of nuclear power systems often lead to prolonged construction periods and high construction and operational costs. An alternative approach to ensure operational safety is through better sensing and control schemes.

Nuclear reactor cores are arguably the most challenging of artificial environments. High temperatures and strong neutron fluxes at levels of  $1 \times 10^{14}$  n/cm<sup>2</sup>/s essentially put most of sensor devices out of operation. Currently, thermocouples are probably the only reliable temperature measurement devices for in-core applications. Since the 1990s, researchers have been exploring the use of optical fiber sensors for in-core monitoring for nuclear power systems [1]. Well known for their resilience in harsh environments [2], fiber Bragg grating (FBG) sensors and distributed fiber sensors can perform multiple simultaneous measurements including temperature, strain, pressure, water levels, and chemical sensing with high spatial

resolutions. This makes FBG sensors attractive sensing devices for nuclear energy applications.

Study of the behavior of various types of FBGs in ionizing radiation environment has spanned for over two decades [3]. Probably the most comprehensive studies are from Fernandez and Gusarov et al., who reported their experiments on FBG sensors in harsh nuclear core environments at the BR1 and BR2 reactors (SCK.CEN) from 1999 to 2008. In 2002, they reported the use of FBGs in various optical fibers, especially photosensitive fibers and telecommunications fibers for online temperature monitoring in low neutron flux ( $\sim 10^{11}$  n/cm<sup>2</sup>/s) and high neutron flux ( $\sim 10^{14}$  n/cm<sup>2</sup>/s) environments. Moderate gamma irradiation was also presented in those studies [4,5]. FBG sensors reported in these studies were irradiated at low temperature from 10 to 80°C, while FBGs endured various radiation doses up to 160 MGy of gamma radiation and a total fast neutron fluence ( $> 1$  MeV) up to  $1.47 \times 10^{17}$  n/cm<sup>2</sup>. After comparative studies using a thermocouple as a reference, it was reported that FBG sensors can measure temperature in those environments with a 3°C accuracy. Studies carried out by Fernandez and Gusarov et al. reveal that both optical fiber materials and FBG sensor fabrication process have great impacts on performance of FBG under these harsh conditions [6–10]. Fielder et al. [11] also claimed an 87% survival rate of FBG sensors in neutron/gamma radiation studies, where FBG fabricated in Ge-doped and B/Ge co-doped fibers endured hours of fast neutron flux ( $1 \times 10^{13}$  n/cm<sup>2</sup>/s) irradiation with accumulated neutron fluence of  $\sim 5 \times 10^{19}$  n/cm<sup>2</sup>, and  $\gamma$ -irradiation of  $2 \times 10^3$  MGy. Recently, Remy et al. [12] used FBG sensors to measure the longitudinal compaction effect on pure silica core and F-doped core samples exposed to fast neutron fluences of  $\sim 4.76 \times 10^{19}$  n/cm<sup>2</sup> at 291°C by measuring the radiation-induced length changes, namely the longitudinal length shortening of the fiber samples.

In this paper, we report in-core studies of FBG sensors at radiation levels similar to those occurring inside commercial nuclear reactors. FBG irradiation tests were performed at  $>600^\circ\text{C}$  with fast neutron fluxes above  $1.2 \times 10^{14}$  n/cm<sup>2</sup> /s for a 55-day continuous irradiations with  $5.7 \times 10^{20}$  n/cm<sup>2</sup> accumulated dose, at least a 10-fold higher dose than previously reported. To evaluate the potential capability of the fiber sensors to monitor reactor anomalies, multiple events were implemented during the irradiation to create abrupt changes of reactor temperatures and reactor powers. FBG responses to these abnormal conditions were characterized to assess thermal-optic properties of FBGs at different stages of irradiation and their temporal response during abrupt temperature changes. Experimental results presented in this paper provide a quantitative evaluation of FBG performance in commercial reactor cores. It also provides cues on how to mitigate FBG property drifts in reactor cores in order to improve both reliability and accuracy of FBG sensors for in-core applications.

## 2. Fiber selection, FBG fabrication, and experimental setup

The in-core radiation experiments reported in this paper were carried out in the MIT nuclear reactor lab. Given the limited space for sensor insertion, two types of optical fibers were selected for the experiment. These two optical fibers were selected based on previous literature studies on radiation-hardened fibers under both gamma and neutron irradiation. They were also selected based on the cost of fibers for potential large scale deployment. These two fibers include pure-silica random air-line (Corning's RAL) fibers and pure silica core, F-doped cladding single-mode fibers (Corning's Vascade) [13]. According to Morana et al [14], F-doped single mode fibers exhibited the lowest radiation-induced attenuation (RIA) at 1550 nm operation, in a study where fs-FBGs inscribed on F-doped, pure-silica core, and Ge-doped fibers were exposed to an accumulated gamma dose of 1 MGy. However, upon exposure to radiation, F-doped fibers had shown a slightly larger Bragg wavelength shift (BWS) towards the blue ( $-0.03\text{pm/kGy}$  for F-doped) compared to pure silica core fibers ( $-0.02\text{pm/kGy}$  for pure silica core). Ge-doped fibers exhibited by far the largest radiation-

induced BWS by approximately two order of magnitudes, which is undesirable for harsh environment sensing.

The pure-silica RAL fiber used in this paper is a nano-engineered optical fiber. The fabrication process is similar to Corning's ClearCurve fiber [15,16] where the fiber was fabricated using outside vapor deposition (OVD) process. A pure silica core cane was inserted into a silica soot blank made with the OVD process to form a preform. The preform was consolidated in a consolidation furnace at a pressurized nitrogen atmosphere around 1450 °C to form a glass cladding containing air bubbles. The preform was then drawn into fiber. During the draw process, the air bubbles were stretched into thin elongated airlines. The optical confinement of the guided mode within the fiber was achieved by the surrounding random air-line structures with a lower average refractive index. Comparing with other air-line microstructural fibers, RAL fibers can be made at much lower cost. Figure 1(a) shows a scanning electron microscope (SEM) cross-section photo of the RAL fiber, where the 8 μm diameter fiber core is surrounded by a random air-line ring 45 μm in diameter to provide optical confinement. Figure 1(b) shows detailed air-line distributions in the fiber cladding. Size of air-line ranges from 15 nm to 1 μm. The size and distribution of the air-line can be controlled by the nitrogen pressure during the fiber preform consolidation process.

The pure silica core fibers are commonly known to have low susceptibility to RIA and hence are the most radiation resistant fibers, especially in operation in near IR range [17]. The entire RAL fiber is made of a single fused silica material with identical thermal expansion coefficient in both fiber core and cladding regions. Both fiber core and cladding also have similar responses under both neutron/gamma radiation. Thus, it is conceivable that the fiber will have even better resistance under radiation exposure. Comparing with other radiation hardened pure silica fibers such as photonic crystal fiber [18], which is also ideally suited for FBG inscription [2], RAL can be manufactured at much lower cost.

To fabricate the Bragg grating in the RAL fiber, a Ti:sapphire regenerative amplifier operating at a central wavelength of  $\lambda = 800$  nm was used. The fs-beam diameter was  $\sim 7$  mm at the  $1/e^2$  level. The full width at half maximum (FWHM) transform-limited width of the pulses was  $\sim 80$  fs, as measured using non-collinear auto-correlation. However, the pulses were pre-chirped to 500 fs in order to facilitate Type II-IR grating formation [19] and the associated nano-grating formation [20]. The pulse repetition rate was kept at 5 Hz. The linearly polarized laser pulses were focused into the fiber core using a 12 mm focal length plano-convex acylindrical lens after passing through a silica phase mask, which has a 3.21 μm pitch. The fiber was positioned approximately 300 μm away from the phase mask along the beam propagation direction. The acylindrical lens was dithered  $\pm 10$  μm at 0.1 Hz with a piezo actuator in order to scan the beam across the fiber core. The resulting grating structure produced a high-order resonance at  $\sim 1525$  nm in the telecom band as shown in Fig. 1(c). FBGs were inscribed in 25 m section of fibers. The locations of the 1 cm long FBGs are approximately 3.5 cm from one end of the fibers.

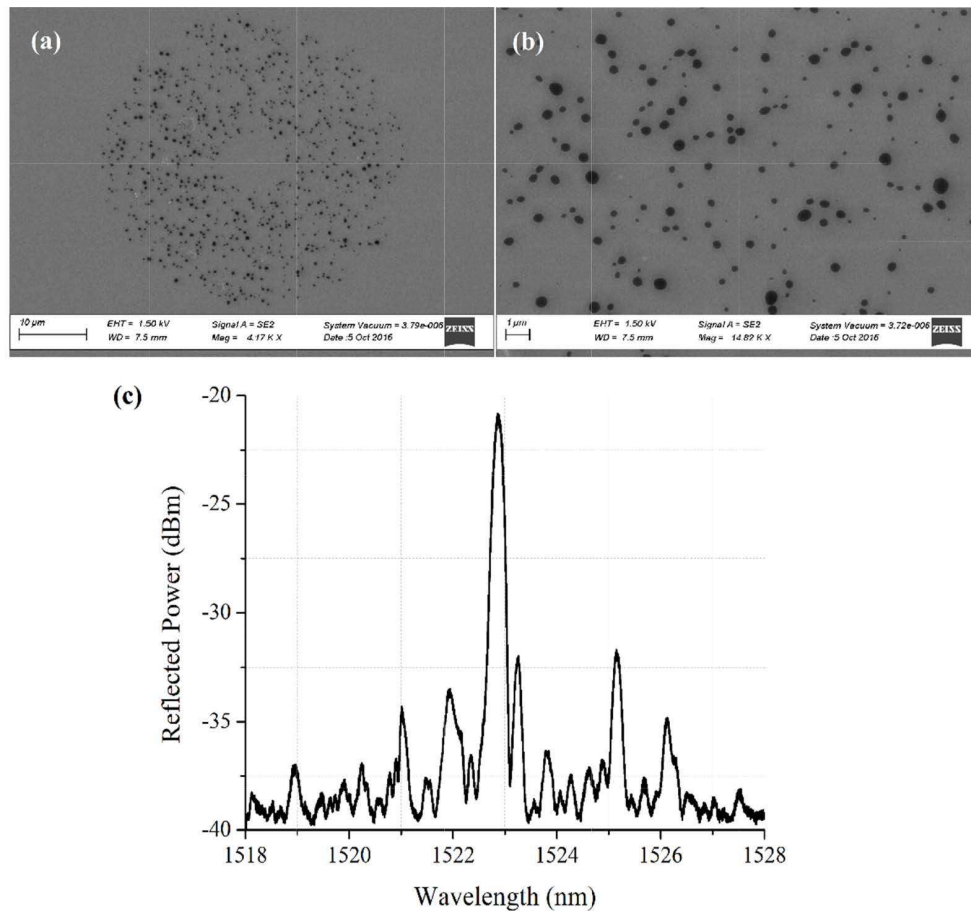


Fig. 1. (a) Cross-sectional microscopic image of the pure silica-core, random-airline cladding fiber of 125  $\mu\text{m}$  diameter. (b) SEM image of the core and random air-lined cladding of the fiber used. (c) FBG reflection profile at room temperature before exposure to neutron flux.

The sensor section of the fiber was slipped into a 6 m long 316 stainless-steel tubing with an outer diameter of 1.59 mm (1/16"), and a wall thickness of 0.25 mm (0.010") for protection and mechanical support of the sample as it descends into the reactor core. The rest of the fiber, which was not subject to any radiation outside the reactor, was sheathed with polyvinylchloride (PVC) tubing. One end of the stainless-steel tube was sealed by welding in argon gas ambient, while the other end of the stainless steel tube was left open to allow the fiber to be fusion spliced to a fiber patch cable with angled physical contact connector to connect with an FBG interrogation system. The FBG interrogation system comprised a TUNICS T100S-HP tunable laser and a CT400 optical switch (both from Yenista Optics) with four interrogation channels. FBG spectra were recorded every 20 seconds as wavelengths of the tunable laser were swept in the range from 1440 nm to 1640 nm with a wavelength resolution of 2 pm.

The MIT reactor (MITR) is a 6 MW light water-cooled, heavy water-reflected reactor with in-core positions for flow loops and instrumented experiment facilities. The core design provides a high power density with a neutron flux and spectrum similar to that of a typical light water power reactor. MITR operates 24/7 with 10-week cycles; typical in-core experiments will operate under steady-state conditions for the duration of each cycle. The fibers are irradiated in MITR's In-Core Sample Assembly (ICSA) facility. The ICSA consists

of a dry, pressurized (inert-gas filled) Grade 2 titanium (ASTM Grade-2) thimble that extends from the bottom of the reactor core to the top of the reactor primary core tank, and permits simplified installation of instrumented experiments desiring temperatures up to 900°C. The experiment capsule and instrumentation leads are all contained within this thimble and are routed at the top through pressure fittings and out of the reactor biological shielding. The heating in this facility is supplied entirely by nuclear heating of the materials under neutron and gamma irradiation, with some fine control available by manipulating the ratio of helium to neon in the facility cover gas. The temperature is actively monitored by multiple thermocouples within the core and feeds back into the gas control system, generally permitting  $\pm 2^\circ\text{C}$  stability during the cycle. Local temperatures are set by the reactor power, materials, and geometry of the heat transfer pathway – the ultimate heatsink is the 50°C reactor primary coolant flowing at the exterior of the ICSA thimble.

Figures 2(a) and 2(b) show a photo and 3D schematic sketch of the test capsule which is placed inside the ICSA thimble. It consists of a graphite sample holder in a 20.5 cm long grade 2 titanium cylinder cup. Stainless tubes containing various fiber sensors are inserted in 4 holes drilled into the graphite sample holder as shown in Fig. 2(a). Three K-type 1/16” thermocouple with Inconel sheaths (from Omega) were also inserted into the reactor core to perform temperature measurements at three different locations in the reactor core region. The locations of the thermocouples are  $-18\text{ cm}$ ,  $-12.5\text{ cm}$ , and  $-5\text{ cm}$  from the center of the titanium cup. The titanium cup, which was placed on a grade 2 titanium pedestal or spacer, was positioned in the middle section of the reactor core to receive the maximum neutron flux.

The neutron flux profile in the reactor core at 5.6 MW, where the test capsule was located, is shown in Fig. 2(c). The test capsule, which is depicted in the figure using a grey bar, is placed in the region with the maximum fast neutron flux, which are in excess of  $1.2 \times 10^{14}\text{ n/cm}^2/\text{s}$  for fast neutrons with  $>0.1\text{ MeV}$  kinetic energy and  $0.6 \times 10^{14}\text{ n/cm}^2/\text{s}$  for fast neutrons with  $>1\text{ MeV}$  kinetic energy.

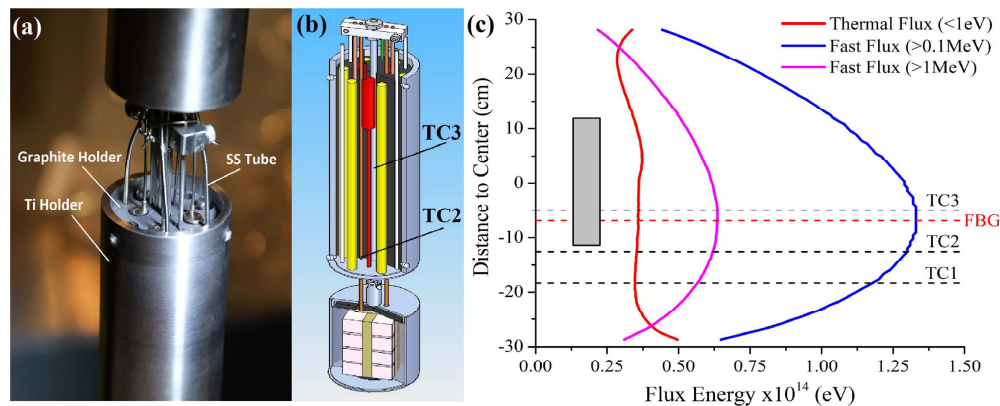


Fig. 2. (a) Stainless-steel tubes with fiber sensor samples and thermocouples inside, inserted into the capsule to be lowered into the reactor core. (b) A 3D schematic of the sample holder capsule that shows the positions of the fiber samples and thermocouples. (c) The neutron fluxes are also plotted to show their spatial profiles relative to the center of the capsule with the three thermocouples locations marked. The Ti capsule is represented on the figure by a grey rectangle.

### 3. Results and discussion

When the experiment commenced, the capsule temperature was raised by  $50^\circ\text{C}$  from room temperature at the first day allowing a test for the response of the sensors before exposure to neutron flux and to confirm that the sensors were safely and accurately inserted inside the nuclear reactor core. The reactor power was then gradually raised over a period of 3 days to be kept steady at 5.62 MW with the capsule reaching a final temperature of  $622^\circ\text{C}$  with a

combination of nuclear heating and helium/neon regulation. Figure 3(a) shows the FBG spectra every 5 days during the test for FBG in RAL fibers. Figure 3(b) shows the spectra of FBG inscribed on Vascade fibers from Day 0 to Day 7. The FBGs in Vascade fibers were damaged after 7 days in the reactor. All data presented thereafter was acquired from FBG in RAL fibers. To simulate FBG sensor behaviors during various reactor anomaly scenarios, several events were staged to assess the response of the FBG prolonged neutron radiation at various accumulated fluences. The reactor power and the capsule temperature measured by TC3 are presented in Fig. 3(c). Reactor power was reduced to 4 MW and 0 MW at Day 18 and Day 32, respectively. A small reactor power reduction also occurred at Day 41 from 5.6 MW to 5.59 MW. This small reactor power reduction did not have significant impacts on FBG. An additional reactor event also occurred at Day 36 as shown in Fig. 3(d), which caused a temporal drop of the FBG wavelength. It is not clear what was the cause of this event. We therefore did not include this event for subsequent data analysis. The temperature and reactor power was then increased at various rates. High-temperature performance of FBG inscribed on this RAL fiber by the femtosecond laser was confirmed independently without radiation [21]. In these experiments, no degradation in reflectivity of the FBG was observed after 5 days at 800°C. The test temperature of 800°C was significantly higher than the reactor temperature of 620°C.

The FBG peak wavelength and reflectivity, measured from peak to baseline, were recorded every 20 seconds. The overall radiation effect on the FBG wavelength and strength is shown in Fig. 3(d). Although reactor anomalies affect the FBG performance, the overall trend of the radiation effect is to cause a blue shift of the FBG resonant wavelength. At constant temperatures (622°C) and neutron flux (5.6 MW), the FBG wavelength drifts slowly towards shorter wavelength, with an average wavelength drift rate of 0.096 nm/day. The FBG wavelength drifts appear to be linear to the accumulated neutron flux. Over the test period of 55 days, FBG wavelength shifted 4.47 nm towards the shorter wavelength. This is consistent with the previous observation of irradiation effects on FBG under gamma and x-ray radiation, as prolonged irradiation (accumulated dosage > 100 kGy) produce blue BWS [3,22]. Although FBGs behavior can be qualitatively explained, the lack of models that accounts fully for the underlying physics governing the behavior of various types of FBGs in radiation environments remains a problem [3,4].

The radiation also weakened the FBG strength. The grating used in these experiment has ~20% (~1 dB) peak reflectivity. The reduction of FBG strength could be the combined effect of radiation-induced absorption and loss of reflectivity of the FBG. On average, during the first 30 days of radiation, the FBG amplitude dropped by 0.125 dB/day, or a reduction of 0.12 dB per  $1.0 \times 10^{19}$  n/cm<sup>2</sup> accumulated fast neutron flux, which is plotted together with the FBG wavelength shifts in Fig. 3(c). However, the reduction of FBG strength appears to saturate as the test progressed. Overall, the FBG strength drops by 6 dB over a period of 55 days of active radiation.

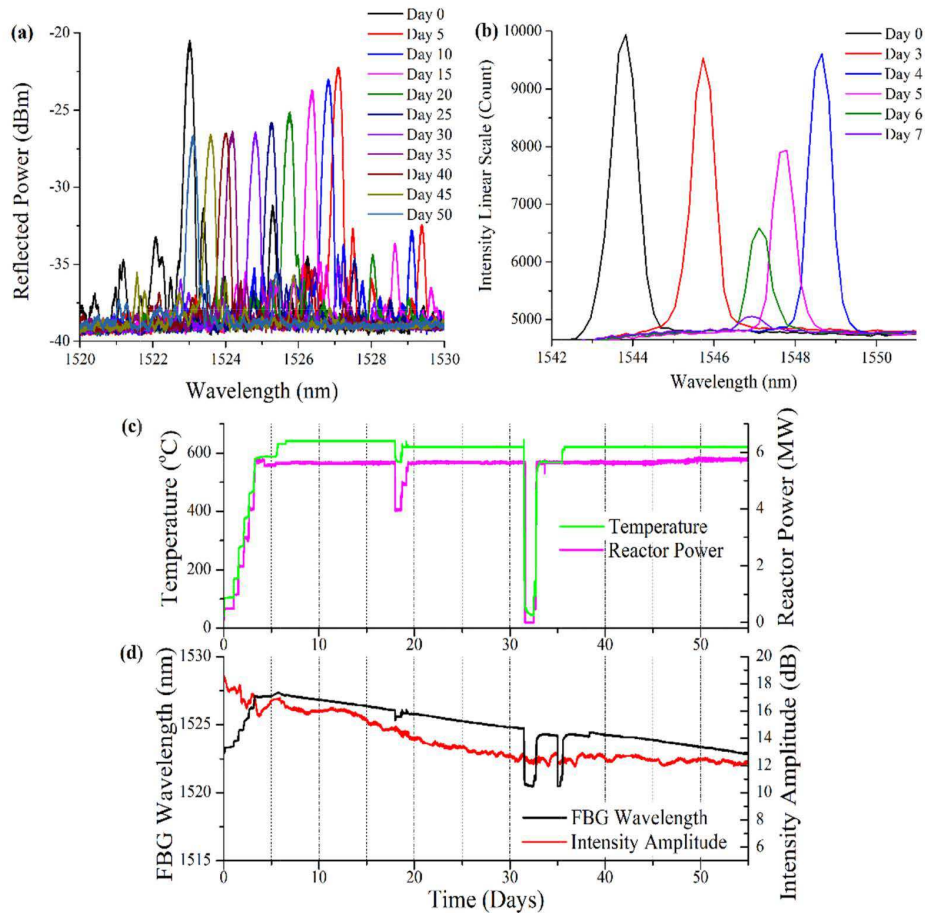


Fig. 3. The FBG wavelength peak initially at Day 0 and at different times with different temperatures and cumulative neutron fluences for the FBG inscribed on the (a) RAL and (b) Vascade fibers. The in-core (c) temperature measured by TC3 and reactor power profile in the first 55 days of nuclear reactor operation, and (d) the RAL FBG response in the form of wavelength and intensity amplitude shifts. The FBG peak wavelength systematic shift due to neutron radiation induced index (RII) changes at constant temperature. The intensity peaks also slightly drop due to the effect of RIA.

Due to three simulated anomaly interrupts of reactor operations at Days 18, 32, and 41, reactor power was varied to 4 MW, 0.1 MW, and 5.59 MW and 0 MW, respectively, from the targeted 5.6 MW at steady state. Behaviors of FBG were also influenced by these interrupts. Results are presented in Figs. 4(a)-4(d). The interrupts of the reactor operation have impact on both FBG wavelength and FBG strength. The continuous irradiation of FBG from Day 6 to Day 18 produced 1.2 nm FBG wavelength blue-shift from 1527.27 nm to 1526.08 nm. The FBG shift follows a linear relationship with the accumulated neutron dosage or irradiation time. This amounts to an FBG linear shift rate of  $-0.096$  nm/day. This wavelength shift rate remains largely consistent without significant saturation. During the subsequent constant irradiation periods between Day 22 and Day 31, Day 38 and Day 41, and Day 42 and Day 55, FBG wavelengths shift rates are measured to be  $-0.090$  nm/day,  $-0.098$  nm/day, and  $-0.101$  nm/day, respectively. FBG wavelength shifts were not characterized during the nuclear power interrupts. This is because the power profiles during the interrupts are complex and relatively short. The relative steady FBG wavelength shift summarized in Table 1 suggests that it could

come from a single dominating underlying mechanism. This is consistent with previous reports on the radiation effects on FBG under gamma and x-ray radiation [3,22]. A linear and steady FBG wavelength drift might be mitigated or calibrated on-the-fly to improve the FBG measurement accuracy for static measurement applications (e.g. temperature or strain). For example, a temperature insensitive in-fiber interferometer might be used to calibrate the radiation induced index (RII) change. On the other hand, irradiation-induced FBG peak reduction shows strong signs of saturation. During the first period of steady radiation between Day 6 and Day 18, FBG peak reduced by 2 dB with a  $-0.136$  dB/day decay rate. The FBG peak decayed at a lower rate during the second period of steady radiation between Day 22 and Day 31 at  $-0.113$  dB/day. The decay rates show strong saturation after 38 days with  $-0.04$  dB/day and  $-0.023$  dB/day during the last two steady irradiation periods, respectively. Intensity amplitudes of the FBG peaks are reduced by less than 0.6 dB between Day 38 and Day 55.

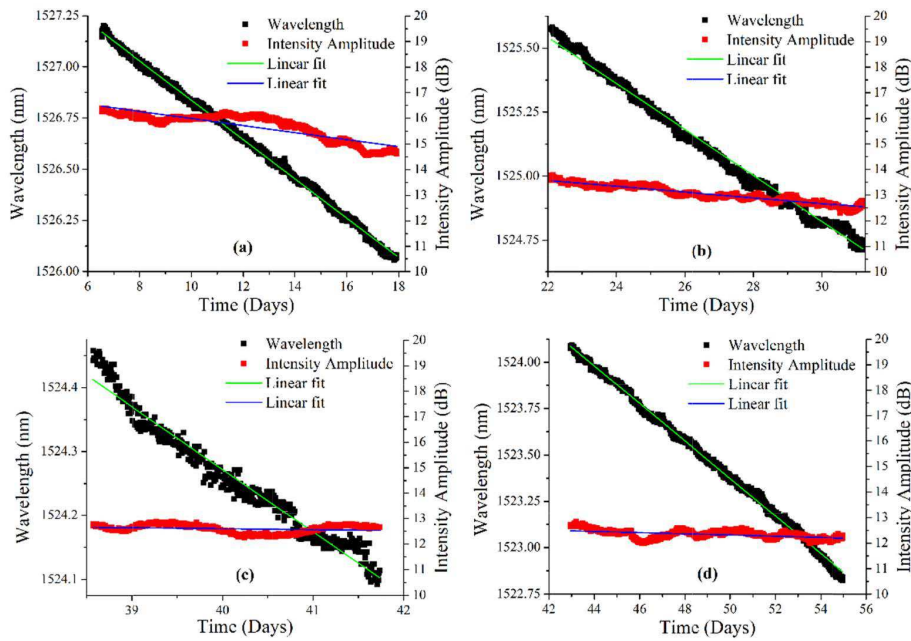


Fig. 4. FBG peak wavelength systematic shift due to neutron flux RII at constant temperature. The intensity peaks also slightly drop due to the effect of RIA.

Table 1. Linear fit characteristics Wavelength drift with neutron flux at constant temperature

Time period (Days)	Reactor Power (MW)	Temperature (°C)	Wavelength Slope or Drift rate (nm/day)	Standard Error in Slope $\times 10^{-4}$ (nm/day)	R-square	Intensity Amplitude Slope or Drift rate (dB/day)	Standard Error in Slope $\times 10^{-3}$ (dB/day)	R-square
6.53- 17.93	5.62	641.56	-0.096	1.167	0.998	-0.1360	1.940	0.750
22.10-31.18	5.63	621.33	-0.090	1.523	0.994	-0.1130	0.672	0.932
38.58- 41.74	5.64	621.51	-0.097	8.663	0.965	-0.0403	8.180	0.048
42.87- 54.97	5.70	621.50	-0.101	1.240	0.997	-0.0232	0.982	0.243

To evaluate FBG responses to reactor anomalies while temperature and reactor power levels experience abrupt changes, a number of events were staged on Day 18, 32, and 41.

During these staged reactor anomalies, reactor power and temperature were raised and reduced at various steps for different periods of times, which creates opportunities to evaluate thermal optic properties of the FBG at various stages of neutron irradiations and different temperature and radiation flux conditions. Some of the transient responses of the FBGs are shown in Figs. 5(a) and 5(b). Results presented in Fig. 5(a) show a staged event while temperature and reactor power was fluctuated several times between 110 and 160°C and 0.5-1 MW, respectively. This was designed to test responsivity of FBG sensors at low temperatures. The temperatures presented in Figs. 5(a) and 5(b) were measured by a thermocouple (TC3 in Fig. 2(b)). Figure 5(b) shows the temporal responses of FBG sensors for another event while the reactor temperature was raised stepwise from 165 to 540°C, and correspondingly the reactor power from 1 to 5.5 MW, while observing the FBG wavelength shift that mimics the change in the aforementioned parameters. The FBG wavelength responses to reactor power changes presented in Figs. 5(a)-5(b) are compared with the thermocouple measurement results. If FBG wavelength shifts are directly and linearly related to reactor temperature changes under intense neutron flux, it is interesting to note that FBG wavelength has faster response to the reactor power changes than those measured by the thermocouple devices as the calculated time constants for the sensors' thermal responses were 239.3 seconds for the FBG sensor, and 269.6 seconds for the thermocouples. This is more pronouncedly illustrated in Fig. 5(b). Given that thermocouples are the only temperature measurement devices within the reactor cores, it is not clear what is the cause of these different response time.

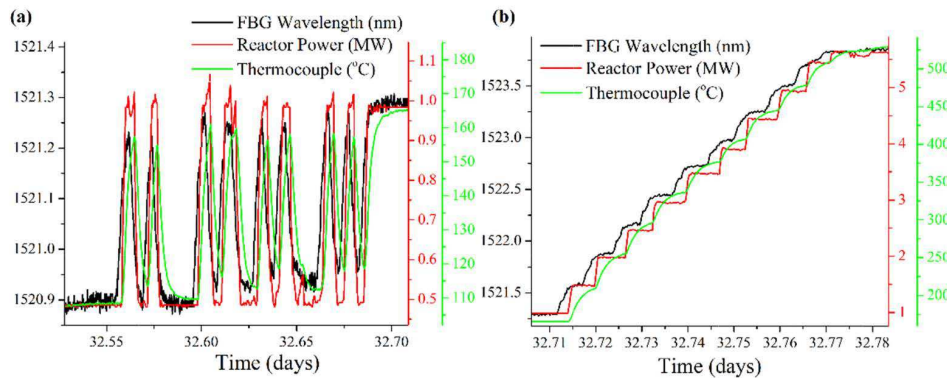


Fig. 5. Different events (a) and (b) were staged by varying the reactor power and temperature inside the reactor core to study the response of the FBG point sensor noted as the FBG wavelength shifts.

To evaluate FBG temperature sensitivity coefficients at different stages of irradiation, four temperature cycles were executed and plotted in Figs. 6(a)-6(d). FBG wavelength changes vs temperature was recorded when the reactor temperature was gradually dropped before quick restoration to the target 622°C. Figures 6(a) and 6(b) show FBG wavelength changes vs. temperature changes during events occurred between Day 32 and Day 33. Figures 6(c) and 6(d) show FBG wavelength changes vs. temperature changes recorded on Day 55, when two events were staged for FBG temperature sensitivity coefficient measurements. All of the measured data are linearly fitted to evaluate the FBG sensor's thermo-optic coefficient that would allow calibration of the sensor and conversion of FBG wavelength shifts to temperature readings. The wavelength changes were measured with respect to the initial wavelength at the start of each cycle, taken at constant temperature and neutron flux. The fitting specifications and results are also summarized in Table 2. The results show a changes in the temperature sensitivity coefficient due to irradiation. Prior to neutron radiation, the FBG temperature sensitivity coefficient is 14 pm/°C. Prolong radiation has reduced the FBG temperature coefficient to 5.97 pm/°C at Day 55.

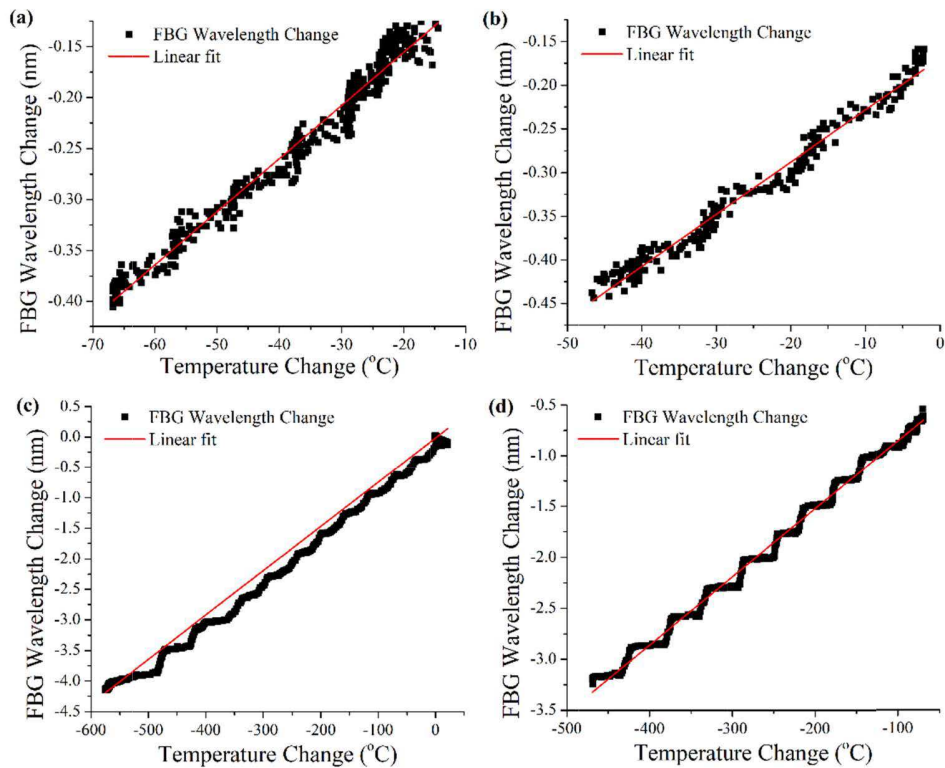


Fig. 6. FBG wavelength shifts as plotted against temperature changes in four different temperature cycles carried out in (a) Day 32, (b) Day 33, and two events in (c), (d) Day 55. The results were linearly fitted to obtain the temperature sensitivity coefficient of the FBG sensor.

Table 2. Linear fit characteristics Wavelength variation with temperature at constant reactor power

Day	Temperature Sensitivity Coefficient $\alpha_T$ (pm/°C)	Standard Error in $\alpha_T$ (pm/°C) $\times 10^{-3}$	R-square
0-4	14.02	1.82	0.932
32	7.25	6.47	0.998
33	6.70	12.90	0.995
55	5.22	38.84	0.972
55	5.97	61.18	0.977

#### 4. Summary and conclusion

This paper presents nuclear irradiation experimental results of temperature-stable FBG sensors fabricated by a femtosecond laser in pure silica random airline fibers. The results show that when appropriate fibers are chosen and suitable laser fabrication techniques are implemented, FBG sensors can survive extreme environments of the nuclear reactor cores under intense gamma and neutron irradiation at high temperatures. The FBG peak decay stabilizes after approximately 34 days of irradiation. However, the FBG wavelength shows a consistent drift toward shorter wavelength at almost constant linear rate of  $-0.1$  nm/day. The reduction in grating strength is related to a reduction in the index modulation while the wavelength shift is due to a change in the average index of the glass under neutron irradiation. The use of FBGs for static measurement could be impacted by this linear FBG wavelength

drift. A self-calibration method might be needed for FBG to perform static measurements such as absolute temperature measurements. FBG Wavelength drift and changes of the FBG temperature sensitivity coefficients induced by strong radiation present significant challenges to use FBG to perform static measurements. Therefore, applications of FBG, in current forms, might be limited by these radiation-induced parameter drifts unless an in-pile calibration technique can be developed. On the other hand, results presented in Table 2 shows that after initial large changes of FBG properties, FBG temperature sensitivity coefficient tends to stabilize. A radiation-harden fiber with multiple FBG could be used to detect significant temperature swings and temperature profile changes over a short period of time. Radiation resilient FBGs presented in this paper can also be used to perform dynamic measurements such as distributed acoustic and vibrational measurements in the reactor core while FBGs are used as reflectors. In summary, results presented in this paper reveal that temperature-stable Type-II FBGs fabricated in radiation-hardened fibers could survive harsh in-pile conditions. Despite large parameter drift induced by strong neutron radiation, further engineering and innovation on both optical fibers and fiber devices could lead to useful fiber sensors for various in-pile measurements to improve safety and efficiency of existing and next generation nuclear reactors.

### **Funding**

U. S. Department of Energy (M3CA-14-PA-PITT-0702-0320 and FE-0028992); Nuclear Science User Facilities grant (15-8489).

### **Acknowledgments**

M. A. S. Z., M. W. and K. P. C. are supported in part by the U. S. Department of Energy grants M3CA-14-PA-PITT-0702-0320 and FE-0028992 and by an appointment to the National Energy Technology Laboratory Research Participation Program, sponsored by the U.S. Department of Energy and administered by the Oak Ridge Institute for Science and Education. This work is also supported by a Nuclear Science User Facilities grant (15-8489).